Climate Dynamics (2019) 52:4567–4581
https://doi.org/10.1007/s00382-018-4418-6

Upper tropospheric ozone transport from the sub-tropics to tropics over the Indian region during Asian summer monsoon

Siddarth Shankar Das[1] · K. V. Suneeth[1] · M. Venkat Ratnam[2] · I. A. Girach[1] · Subrata Kumar Das[3]

Received: 20 November 2017 / Accepted: 7 August 2018 / Published online: 27 August 2018

Abstract
In this study, we investigate the role of the Asian summer monsoon (ASM) anticyclone in the distribution of ozone over the southern India and tropical Indian Ocean. We present the horizontal and vertical structure of ozone in the upper troposphere and lower stratosphere (UTLS) region. The analysis shows that the region within the ASM anticyclone has low ozone, and high tropopause altitude, as compared to the region outside the anticyclone during boreal summer. The southern edge of the ASM anticyclone, i.e. the southern India and tropical Indian Ocean show a remarkably high ozone concentration in the UTLS region during summer. Analysis of daily fields shows that ozone concentration in the upper troposphere over the southern India and tropical Indian Ocean increases with the strength of the tropical easterly jet, which is an outcome of ASM circulation. Different mechanisms responsible for the ozone enhancement in the UTLS region over the tropical Indian region have been discussed in this paper. The in situ ozonesonde observations from six Indian stations also support the space-based Aura-MLS observations, concluding that ASM anticyclone effectively transports ozone from the mid-latitude stratosphere to deep tropics. Shear generated turbulence and mixing in the vicinity of easterly jet also likely to play a minor role in the local ozone distribution.

Keywords Ozone · Tibetan Plateau · Asian Summer Monsoon · Aura-MLS · COSMIC

1 Introduction

The stratospheric ozone (O_3), which maximizes between 25 and 30 km altitude, regulates the amount of ultraviolet (UV) radiation received on the Earth's surface. In addition to it, tropospheric ozone is an important greenhouse gas and acts as an oxidant, and thus plays a significant role in the climate system (Pan et al. 2015). The enhancement in the tropospheric ozone has major consequences on living beings, as it acts as a toxic agent among air pollutants. Tropospheric ozone will increase either due to the in situ photochemical formation associated with lightning, advection, and anthropogenic activities (e.g. Jacobson 2005, and references therein) or due to the stratospheric intrusion (Wild 2007, and reference therein; Škerlak al. 2014).

An increase in the downward flux of stratospheric ozone-rich air to the troposphere not only enhances the tropospheric ozone but also reduces the stratospheric ozone concentration. The lifetime of ozone reduces once it reacts with the tropospheric constituents. In general, the tropospheric ozone enhancement due to stratospheric intrusions is observed over the middle and high latitudes and is linked with synoptic scale disturbances (Stohl et al. 2003). This is attributed to the dissipation of extra-tropical synoptic waves in the stratospheric region (Holton et al. 1995). Bourqui and Trepanier (2010) have estimated the global tropospheric ozone budget and found that 25–50% sources are from middle-latitude stratospheric intrusion. So far, there are many observational evidences of stratospheric intrusion during (1) cutoff lows (Vaughan and Price 1989), (2) high/low-pressure systems (Davies and Schuepbach 1994), (3) the tropopause folds (Sprenger and Wernli 2003), and (4) a rapid episodic intrusion due to the overshooting convections (Baray et al. 1999; Cairo et al. 2008; Das 2009; Das et al. 2011, 2016a,

✉ Siddarth Shankar Das
dassiddhu@yahoo.com

[1] Space Physics Laboratory, Vikram Sarabhai Space Centre, Trivandrum 695022, India

[2] National Atmospheric Research Laboratory, Department of Space, Gadanki 517112, India

[3] Indian Institute of Tropical Meteorology, Pune 411008, India

b; Zhan and Wang 2012; Jiang et al. 2015; Venkat Ratnam et al. 2016).

There are various studies which show that variability of trace constituents, viz. water vapour (H_2O) (Tian et al. 2011; Randel et al. 2006; Xu et al. 2014), O_3 (Tobo et al. 2008; Gettelman et al. 2004; Zhou and Luo 1994), methane (CH_4), nitrogen oxide (N_2O) (Park et al. 2004), carbon monoxide (CO) (Fu et al. 2006), and aerosol (Lau et al. 2006) are influenced by Asian Summer Monsoon (ASM) anticyclone, centered over the Tibetan Plateau (TP) in the upper troposphere and lower stratosphere (UTLS). The TP acts to enhance the coupling between the subtropical and tropical monsoon circulations (e.g., Wu et al. 2012), and have a significant impact on the intensity of precipitation (e.g., Liu et al. 2012). The ASM anticyclone encompasses a westerly in mid-latitudes and easterly in the tropics (Dunkerton 1995). The presence of ASM anticyclone is the result of elevated surface heating and persistent deep convection over the TP and India during boreal summer (Yanai et al. 1992; Liu et al. 2001; Duan and Wu 2005; Randel and Park 2006; Park et al. 2007; Kucharski et al. 2010). Remarkable horizontal and seasonal variabilities of these minor constituents are attributed to the strong winds and closed streamlines associated with this anticyclone, which act to isolate the air (Randel and Park 2006; Park et al. 2007).

The concept of 'ozone valley' during boreal summer over the TP has been discussed for decades. Various studies have reported that total ozone over the TP is much lower than that over the surrounding areas of same latitudes; thus the TP is known to be an 'ozone valley' (Zhou and Luo 1994; Zou 1996; Tobo et al. 2008). Horizontal transport of ozone from extra-tropics into the tropical tropopause layer (TTL) over the ASM region is examined by Konopka et al. (2010), and Randel and Jensen (2013) using observations and modeling studies. The annual cycle of ozone over the zonally averaged tropical lower stratosphere is studied by Stolarski et al. (2014). Authors found a seasonal maximum during July–August over the Northern Hemisphere (NH) tropics and September–October over the Southern Hemisphere (SH) tropics. Maximum ozone is found in the tropical region of NH than SH. The ozone annual cycle in the TTL is explained by the seasonality of in-mixing and upwelling along with the phases of these two processes (Konopka et al. 2010; Stolarski et al. 2014). In addition to the horizontal transport of ozone associated with ASM circulation, there is also a vertical exchange of these minor constituents between the troposphere and stratosphere. Fadnavis et al. (2010) have made a detailed study of the seasonal characteristics of stratospheric ozone intrusion over the ASM region using satellite observations and modeling. The vertical distribution of tropospheric ozone over the ASM region is studied by Worden et al. (2009). Bian et al. (2012) have carried out in situ measurements of ozone and water vapour over the two locations in TP and the results were well comparable with the satellite observations and modeling studies.

Most of the earlier studies on ozone distributions either focus on the central part of ASM anticyclone (i.e., over the TP) or presented the averaged structure of entire ASM region. These studies do not pay much attention to the exchange of minor constituents in the southern-most part of ASM anticyclone, i.e. over the southern India and tropical Indian Ocean. The purpose of this study is to explore and present the structure, variability, and transport of ozone in the UTLS region over the southern India and tropical Indian Ocean using long-term in situ and satellite observations. In this study, we use ~ 14 years of O_3 and CO observations from Aura-Microwave Limb Sounder (MLS) over the ASM region and ~ 45 (4) years of in situ ozonesonde measurements from three (one) different Indian locations. In addition, we also use 11 years of temperature profiles obtained from the "Constellation Observing System for Meteorology Ionosphere and Climate" (COSMIC) mission data and winds from ERA-Interim reanalysis produced by the European Centre for Medium-Range Weather Forecasts (ECMWF) for mass-flux estimation.

This paper is structured as follows: Sect. 2 briefly describes the data analysis and methodology. Observations are described in Sect. 3, followed by results and discussion in Sect. 4 and finally summary in Sect. 5.

2 Data analysis

2.1 Aura MLS

Profiles of ozone (O_3), water vapour (H_2O) and carbon monoxide (CO) mixing ratios are obtained from Aura-MLS measurements. Water vapour profiles were retrieved from the radiance measurements of ~ 190 GHz rotational line, whereas, ozone and carbon monoxide profiles were retrieved from the radiance measurements of ~ 240 GHz. We use Aura-MLS version 4.2 level-2 data. We constructed monthly mean gridded data of 2.5° × 2.5° from August 2004 to December 2017. This data has a precision of 15–20%, an accuracy of 8–15%, and a minimum of 0.1 ppmv in water vapour measurements. Ozone measurements have a precision of 15–25% and an accuracy of 5%. Carbon monoxide measurements have a precision of 20–25% and accuracy of 30%. The equatorial crossing local time of Aura-MLS is 01:30 AM and 01:30 PM and can provide ~ 3500 profiles per day. A detailed description and data quality can be found elsewhere (Livesey et al. 2015; Lambert et al. 2015; Schwartz et al. 2015).

2.2 GPS-RO COSMIC

The cold-point tropopause (CPT) and lapse-rate tropopause (LRT) altitude (CPT-A/LRT-A) and temperature (CPT-T/LRT-T) are derived from the temperature profiles obtained from the COSMIC mission data. The COSMIC measurements are based on an active limb sounding GPS-Radio Occultation (GPS-RO) technique. The temperature is derived from the refractivity profile obtained from GPS-RO technique. Detailed method and retrieval technique of GPS-RO can be found in Kursinski et al. (1997). A precision of 0.1% is estimated in COSMIC temperature measurements (Alexander et al. 2014). Hajj et al. (2004) estimated a temperature accuracy of better than 0.5 K for individual profiles and 0.1 K for averaged profiles in the UTLS region. We use level-2 temperature profiles (known as 'wetPrf') with 100 m vertical resolution, obtained from COSMIC Data Analysis and Archive Center (CDAAC) for the period December 2006–August 2017. The COSMIC temperature profiles provide global tropopause data with a good accuracy and vertical resolution in any weather conditions (e.g., Randel and Wu 2015). There are ample of studies, where COSMIC temperature profiles are used to explore the global climatology of tropopause from seasonal to diurnal scales (e.g., Kim and Son 2012; Munchak and Pan 2014; Suneeth et al. 2017).

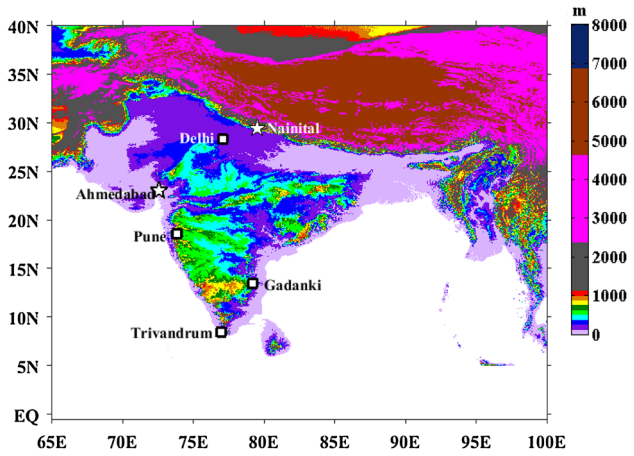

Fig. 1 Topography of South Asia. Ozonesonde stations over India are marked with square boxes (data presented) and stars (data discussed)

2.3 Ozonesonde and radiosonde

In addition to the ozone profiles from Aura-MLS, we use in situ ozonesonde observations over the Indian region. Figure 1 shows the topography map of south Asia along with ozonesonde launching sites (marked with square boxes and stars). Square boxes represent the ozonesonde stations, where the data is used in this paper, and stars represent the ozonesonde stations, where the features are only discussed from the published literature. Table 1 shows the detail of each ozonesonde station and its operating agencies. The ozonesondes launched by the India Meteorological Department (IMD) are modified electrochemical Brewer bubbler ozone sensor (B-M sonde) developed in the Ozone Research Laboratory of the IMD (Sreedharan 1968; Alexander and Chatterjee 1980). The IMD launches ozonesonde every fortnight from Delhi (DEL), Pune (PUN) and Trivandrum (TRI). Indian ozonesondes were compared with Electro Chemical Cell (ECC) sondes and underestimations of 5–10% were found in the troposphere (Kerr et al. 1994; Deshler et al. 2008). The data is collected from 1966 to 2014. There are a few studies which used Indian ozonesondes for estimating the long-term trend in the UTLS region (e.g., Saraf and Beig 2004; Fadnavis et al. 2012). Detailed system descriptions of the Indian ozonesonde can be found elsewhere (Sreedharan 1968; Alexander and Chatterjee 1980). Apart from IMD, other national institutes like Space Physics Laboratory (SPL) at TRI, National Atmospheric Research Laboratory (NARL) at Gadanki (GAD), Physical Research Laboratory (PRL) at Ahmedabad (AHD), and Aryabhatta Research Institute of Observational Sciences (ARIES) at Nainital (NTL) also launched 1–2 years of ECC based ozonesondes (EN-SCI, USA). The uncertainty in the ECC based ozone measurements is 5–10% (Komhyr et al. 1995). These ECC ozonesondes were launched regularly as well as in campaign mode measurements.

Table 1 Details of the ozonesonde observations in India

Station	Latitude (°N)	Longitude (°E)	MSL (m)	Period	Total no. of profiles	Operating agency	References
Nainital	29.4	79.5	1958	2011	48	ARIES	Ojha et al. (2014)
Delhi	28.3	77.1	273	1966–2014	320	IMD	Saraf and Beig (2004)
Ahmedabad	23.03	72.54	50	2003–2007	83	PRL	Lal et al. (2014)
Pune	18.53	73.85	559	1966–2014	303	IMD	Saraf and Beig (2004)
Gadanki	13.5	79.2	375	2010–2014	52	NARL	Raj et al. (2015)
Trivandrum	8.48	76.95	60	1969–2014	268	IMD	Saraf and Beig (2004)

In addition to the fortnight ozonesondes, we also use regular (daily) IMD radiosonde (MK-III) measurements for winds and temperature, which are launched daily at 00 and 12 GMT from DEL and TRI from January 2004 to December 2016. Radiosondes of different make/model were also launched at GAD from April 2006 to April 2016 at 12 GMT. Vaisala RS-80/92 radiosonde were launched during April to August 2006 and afterward Meisei RS-06G/11G were launched from GAD (Nash et al. 2011; Kizu et al. 2018). The temperature sensors Vaisala radiosonde is capacitive wire sensor and the Meisei radiosondes are thermistors. The accuracy of IMD radiosonde is better than 1 K with a precision of ~0.6 K (Chakrabarty et al. 2000). For Vaisala and Meisei model radiosondes, the accuracy is better than 0.5 K with a precision of 0.3 K (Steinbrecht et al. 2008; Kizu et al. 2018).

2.4 ERA-Interim reanalysis

We also used monthly averaged horizontal and vertical winds from ERA-Interim reanalysis produced by the European Centre for Medium-Range Weather Forecasts (ECMWF). The grid resolution is 2.5° × 2.5°. Dee et al. (2011) described the detailed bias correction, accuracy, and limitation of these data sets. Horizontal wind of ERA-Interim shows good correlation with the observation over the tropical Indian latitude (Das et al. 2016c).

3 Observations

3.1 Aura-MLS observations

Figure 2 shows the seasonal mean ozone mixing ratio (OMR) at three different pressure levels (i.e. 82, 100, and 121 hPa), which covers the UTLS region along with wind vectors. We use the terminology 'lower stratosphere' (LS) to the pressure level of 82 hPa, in the 'vicinity of tropopause' (VOT) to 100 hPa, and 'upper troposphere' (UT) to 121 hPa. We observed low ozone (200–300 ppbv) in the equatorial LS region, especially over the NH during December–January–February (DJF) (hereafter boreal winter). Ozone is below 200 ppbv in the VOT over the western equatorial Pacific region. The minimum in OMR during boreal winter

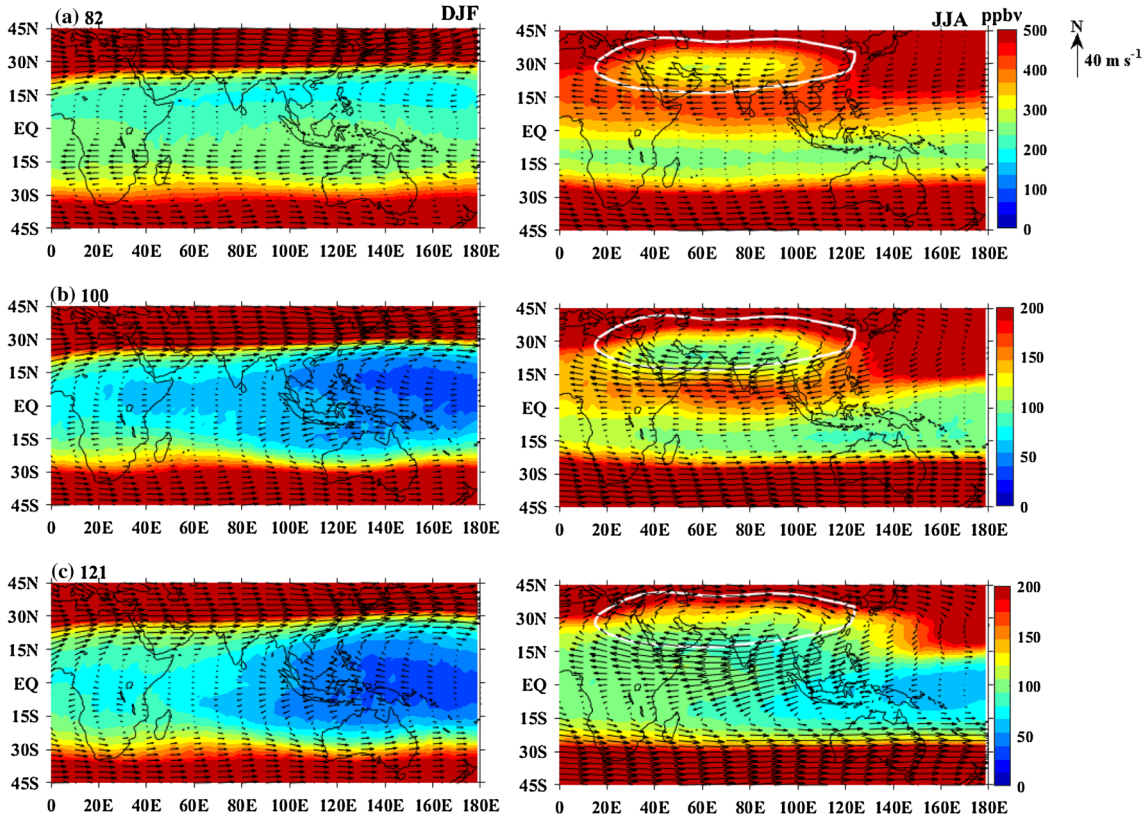

Fig. 2 Longitude–latitude distribution of ozone mixing ratio at **a** 82 hPa, **b** 100 hPa, and **c** 121 hPa observed during boreal winter (left panels) and summer (right panels) averaged from Aug. 2004 to Oct. 2017. Arrows indicate the seasonal mean vector winds averaged from 2004 to 2017 for 70, 100, and 125 hPa in Fig. 2a–c, respectively. White closed contour in the right panels indicate the climatological location of the Asian summer monsoon anticyclone

is attributed to the increased strength of the tropical mean upwelling (Randel et al. 2007). Strong westerly winds (associated with subtropical jet) are observed in the UTLS region over the mid-latitudes of both the hemispheres during winter.

One of the noticeable features of the ASM is the presence of anticyclone associated with the strong heating over the TP during June–July–August (JJA) (hereafter boreal summer). White contour in Fig. 2 (right) indicates the region of ASM anticyclone. Tropical easterly jet (TEJ) is another phenomenon associated with the ASM anticyclone over its southern edge (southern India and tropical Indian Ocean). TEJ is the strong easterly winds observed between the tropopause and 150 hPa (Sathiyamoorthy et al. 2007; Raman et al. 2009). Westerly winds are observed in the northern edge of the anticyclone. It is interesting to note that there is a drastic increase in ozone in the VOT and LS along the path of TEJ during boreal summer. An enhancement of ~ 120 ppbv (~ 200 ppbv) in OMR is found in the VOT (LS) during boreal summer as compared to winter. Over Korea, Kim et al. (2002) have shown the stratospheric air intrusion into the upper troposphere, which is attributed to the strong zonal wind during winter and spring times. Another feature we observed is the decrease in the UTLS ozone inside the anticyclone. However, we do not observe a significant increase in ozone concentration along the path of TEJ over the Indian peninsula in the UT region.

3.2 Ozonesonde observations

It is to be noted that the vertical resolution of MLS ozone measurement is relatively coarse in the tropical UTLS region. Glanville and Birner (2017) have discussed on the kernel averaging at 80 hPa level, which includes 20% contribution from 100 hPa. Thus, we compare the space-borne MLS observations with the in situ ozonesonde observations available from four Indian stations. Figure 3 shows the annual mean removed monthly OMR for the (a) DEL, (b) PUN, (c) GAD, and (d) TRI measured using Aura-MLS (left), and in situ ozonesonde observations (right). The seasonal characteristics of ozone measurements from MLS are comparable with ozonesonde observations. We observed high ozone in the VOT during boreal winter and very low ozone during summer over the DEL. Lal et al. (2014) and Ojha et al. (2014) have also reported low ozone in the VOT

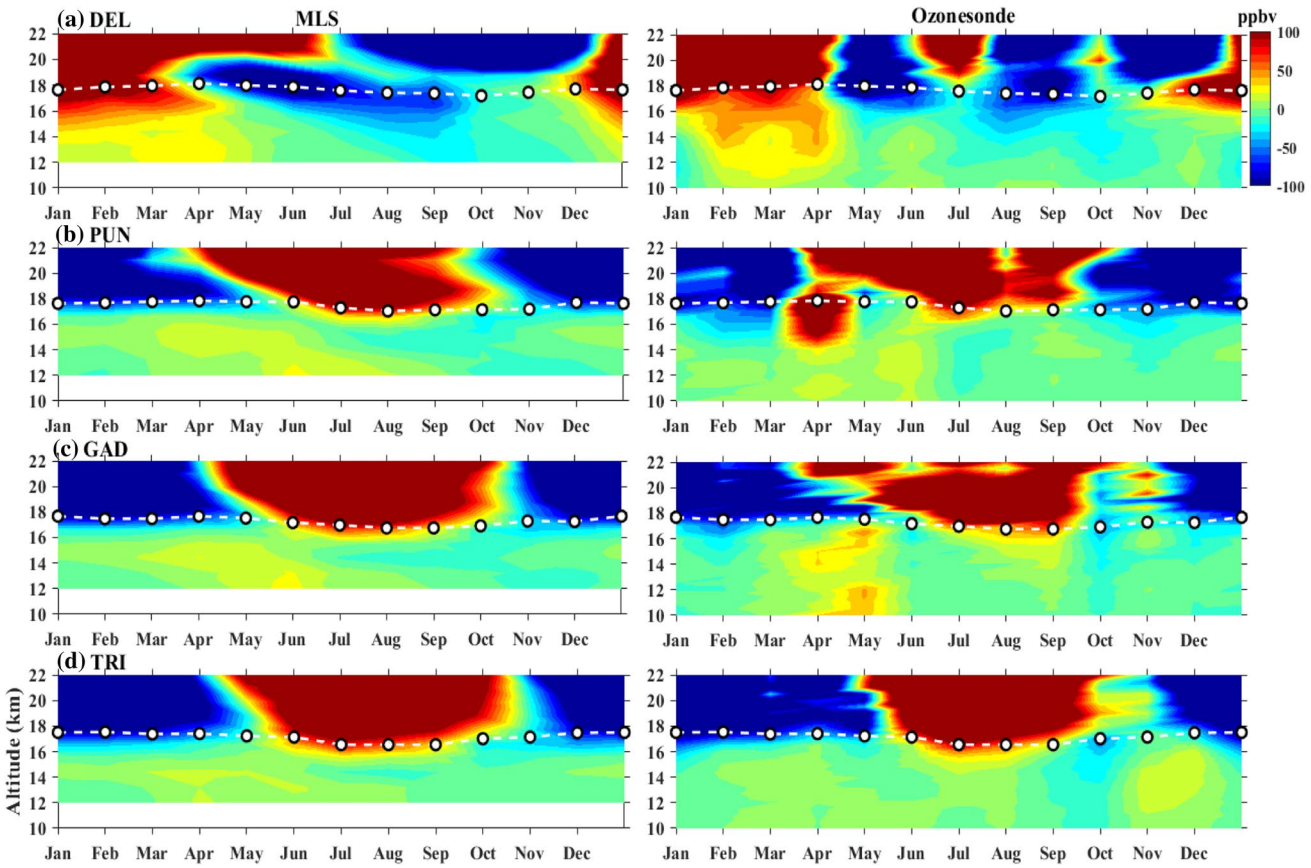

Fig. 3 Annual mean removed monthly vertical structure of ozone mixing ratio for **a** Delhi (DEL), **b** Pune (PUN), **c** Gadanki (GAD), and **d** Trivandrum (TRI) obtained from Aura-MLS (left) and ozonesonde (right) observations. Circles indicate the monthly mean CPT-A determined from the COSMIC temperature profiles averaged of December 2006–August 2017

during summer using ozonesonde observations over the AHD and NTL, respectively. DEL, AHD and NTL stations are inside the ASM anticyclone. In contrast to it, we observe very low ozone during boreal winter and very high ozone during summer over the PUN, GAD, and TRI as a result of reduced tropical upwelling and significant in-mixing. Low CPT-A is also observed over PUN, GAD, and TRI during boreal summer. Raj et al. (2015) reported high ozone concentration during summer over the GAD. The ozonesonde stations at PUN, GAD, and TRI lie in the path of TEJ, i.e., the southern edge of ASM anticyclone. Thus, the enhancement in the ozone (apart from the annual cycle) is noticed in the VOT between the equator and 15°N during boreal summer in both the space-borne and in situ observations.

4 Results and discussion

In order to investigate the influence of ASM anticyclone in the ozone enhancement, we have plotted the global zonal mean removed OMR at 100 hPa superimposed with zonal wind (easterly) contour at 150 hPa (< -25 m s^{-1}), during boreal summer in Fig. 4a. Enhancement of ozone is observed in distinct regions; i.e (1) > 60 ppbv is observed between 140°–180°E and 10°–30°E, and (2) 30–40 ppbv is observed between 50°–100°E, and equator to 10°N. The spatial distribution of ozone enhancement over the Indian peninsula (including the tropical Indian Ocean) and TEJ are coinciding. Further, we plotted the latitude–altitude cross-section of the global zonal mean removed OMR superimposed on zonal wind averaged of 60°E–80°E during boreal summer, as shown in Fig. 4b. The zonally averaged (60°E–80°E) tropopause altitude (CPT-A and LRT-A) is also superimposed in the Fig. 4b. A positive anomaly of ozone is observed between 15.5 and 19 km and between 10°S and 15°N. The observed slanting structure from the upper (NH) to lower (SH) altitude is consistent with the spatial structure of the anticyclone. The TEJ also shows the similar slanting structure from NH to SH (higher to lower altitude) but the core of TEJ (~ 14 to 16 km) and ozone (~ 16 to 18 km) shows a latitudinal shift by 5°. In between the core of TEJ and ozone, the CPT-A and LRT-A, respectively show lower altitude over the tropics.

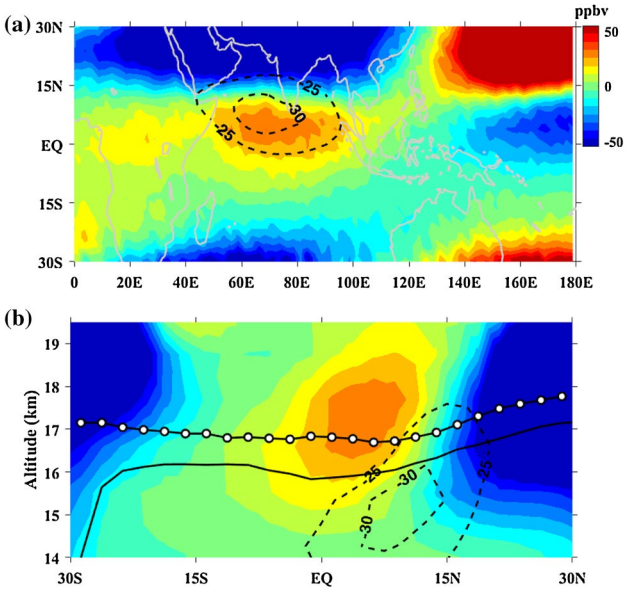

Fig. 4 Global zonal mean removed ozone mixing ratio **a** latitude–longitude distribution at 100 hPa, and **b** latitude–altitude cross-section averaged from 60°E to 80°E during boreal summer. The dashed contours indicate the easterly jet, and black line with and without circles indicate the CPT and LRT altitude, respectively

Further, we estimate the fractional annual cycle of ozone ($O_{3[Fraction]}$) in potential temperature co-ordinate over the Indian peninsula by the following Eq. (1):

$$O_{3[Fraction]} = \frac{O_{3[Individual\ profile]} - O_3}{O_3} \quad (1)$$

where $O_{3[Individual\ profile]}$ is the individual profile of ozone and O_3 is the annual mean of ozone profile. The potential temperature (θ) is estimated using the temperature profile (T) of radiosonde observations, by the following Eq. (2):

$$\theta = T\left(\frac{P_0}{P_z}\right)^{0.286} \quad (2)$$

where P_0 is the standard pressure (1000 hPa) and P_z is the atmospheric pressure at level z. The θ co-ordinate is used instead of pressure–altitude co-ordinate to avoid the seasonality of temperature (e.g., Konopka et al. 2010). Figure 5 shows the fractional annual cycle of ozone averaged of PUN, GAD, and TRI. A high fraction of ozone (0.4–0.5) is observed during boreal summer (including September) between 380 and 430 K. Similar observations are also reported by Konopka et al. (2010) for the near-equatorial ozonesonde observations. Earlier studies suggested that tropical region is isolated from the mid-latitude and in-mixing can be negligible (e.g. Randel et al. 2007). However, Konopka et al. (2010) pointed out that such enhancement of ozone in the upper part of TTL cannot be fully explained by photolytic ozone production and there exists an in-mixing apart from the slow upwelling. Thus, the observed lower stratosphere ozone maximum during summer over the Indian peninsula may be a combination of in-mixing from the mid-latitude stratosphere, and in situ production.

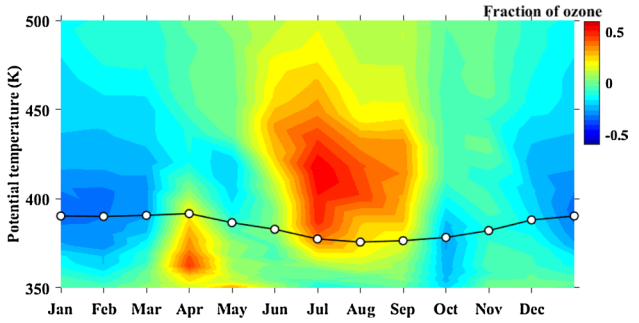

Fig. 5 The fraction annual variation of ozone, averaged for the stations: PUN, GAD, and TRI using ozonesonde observations (see text for details). The black line with circles indicate the CPT-A

4.1 Role of anticyclone in horizontal transport

It is clearly observed in Fig. 2 that there is a horizontal transport from mid-latitude to tropics, following the path of the ASM anticyclone and TEJ. Randel and Jensen (2013) have discussed the role of monsoon circulations in enhancing the transport into and out of the tropics along the anticyclone path. Thus to examine the potential source of observed ozone over the Indian peninsula, we use NOAA's Hybrid Single Particle Lagrangian Integrated Trajectory (HYSPLIT) model (Stein et al. 2015). The meteorological data used for the trajectory calculation is from Global Data Assimilation System (GDAS) with 1° latitude–longitude grids. Figure 6 shows the 10-day backward trajectories on daily basis ending at 16.5 km (i.e., average tropopause altitude) for (a) June, (b) July, and (c) August (2005–2017). The endpoint of the trajectories (shown by a star mark) is taken over the equatorial Indian Ocean (5°N, 70°E) near to the Indian peninsula where higher ozone is observed. The altitude of air parcel along the trajectories is shown by color. This analysis reveals that the observed air masses with high ozone in the UT over the southern India and tropical Indian Ocean are originated from the TP and northern part of ASM anticyclone. The altitude of air parcels is around 17.0–17.5 km (a.m.s.l) over the mid-latitudes of the eastern part of ASM anticyclone, showing the transport of stratospheric air to UT over the southern India and tropical Indian Ocean through isentropic winds.

4.2 Role of turbulence

Figure 7 shows the monthly mean climatology of zonal wind in the UTLS region at DEL, GAD, and TRI averaged from 2004 to 2016. Since we have less than 1 year (during 2016–2017) of observation over PUN, we do not show the same. DEL shows strong westerly wind in the UT, i.e., sub-tropical jet during winter and low wind during summer. GAD and TRI show strong easterly wind i.e., TEJ between 13 and 18 km during summer till September. This strong

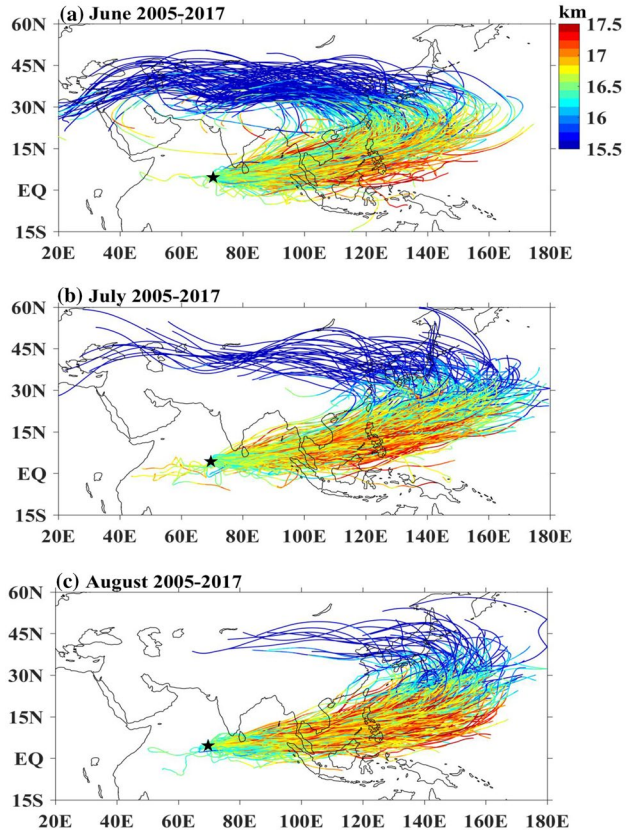

Fig. 6 10-day backward trajectory analysis for **a** June, **b** July, and **c** August for the period 2005–2017 using NOAA's HYSPLIT model (GDAS 1 deg). The end point (5°N, 70°E) of trajectories is shown by a star mark which is at an altitude of 16.5 km. The color of the trajectories shows the altitude (a.m.s.l.) of the air parcel

wind in the VOT can generate turbulence due to the presence of strong wind shear and which may lead to the mixing of stratospheric air with the tropospheric air.

To get further insight, we estimated the stability parameter (N^2, where N is Brunt–Väisälä frequency), square of vertical shear of horizontal wind (S^2) for individual profiles and Richardson number (Ri) using the following Eqs. (3)–(5), respectively and it is shown in Fig. 8.

$$N^2 = \frac{g}{\theta}\left(\frac{\partial \theta}{\partial z}\right) \tag{3}$$

$$S^2 = \left(\frac{\partial u}{\partial z}\right)^2 + \left(\frac{\partial v}{\partial z}\right)^2 \tag{4}$$

$$Ri = \frac{N^2}{S^2} \tag{5}$$

where u and v are zonal and meridional winds. These parameters are estimated for Individual profiles and then averaged

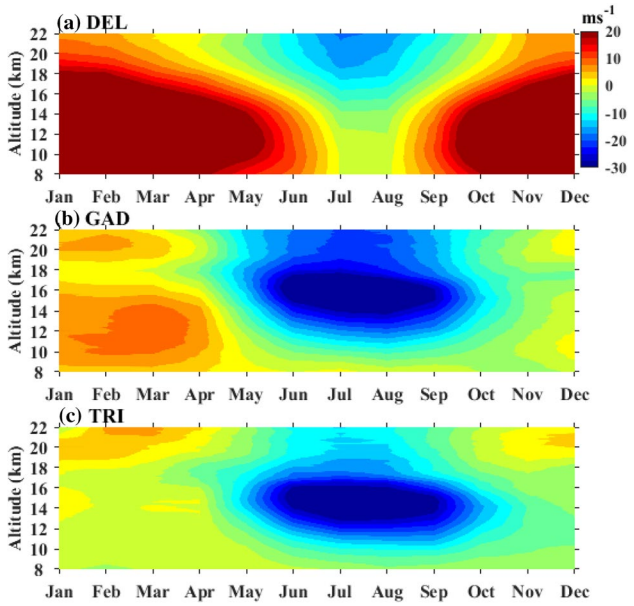

Fig. 7 Monthly mean climatology of zonal wind for the stations: **a** DEL (Jan. 2004–Dec. 2016), **b** GAD (Apr. 2006–Apr. 2017), and **c** TRI (Jan. 2004–Dec. 2016)

for each month. It is interesting to note that enhanced values of stability parameter in the VOT appear during boreal summer as compared to winter over the GAD and TRI. The enhanced value of stability parameter in the VOT region indicates the presence of stratospheric air as the stratosphere is highly stable. This indicates that the tropopause (Fig. 3) (lower stratosphere) has come down to a lower altitude. Corresponding to the enhanced stability parameter, we also observed strong vertical shear of horizontal wind during boreal summer in the VOT over the GAD and TRI, suggesting the presence of dynamic instability. These features are not observed over the DEL during summer. Further, $Ri < 1$ over GAD and TRI during summer, suggests the presence of shear generated turbulence (dynamics instability). $Ri < 0.25$ is generally considered as the critical value for the onset of turbulence. $Ri < 0.25$ is to initiate turbulence, which may persist for the value of Ri as high as 1.0 (Johnson 1975). Nevertheless, a few studies (e.g., Johnson 1975; Murphy et al. 1982) considered $Ri < 1$ as the necessary condition to sustain the wind-shear generated turbulence. This turbulence can participate in the direct vertical mixing of stratospheric air into the upper troposphere. The occurrence of vertical mixing along with the horizontal mixing (filamentation due to differential advection) also likely to contribute some extent in the ozone enhancement near the tropopause.

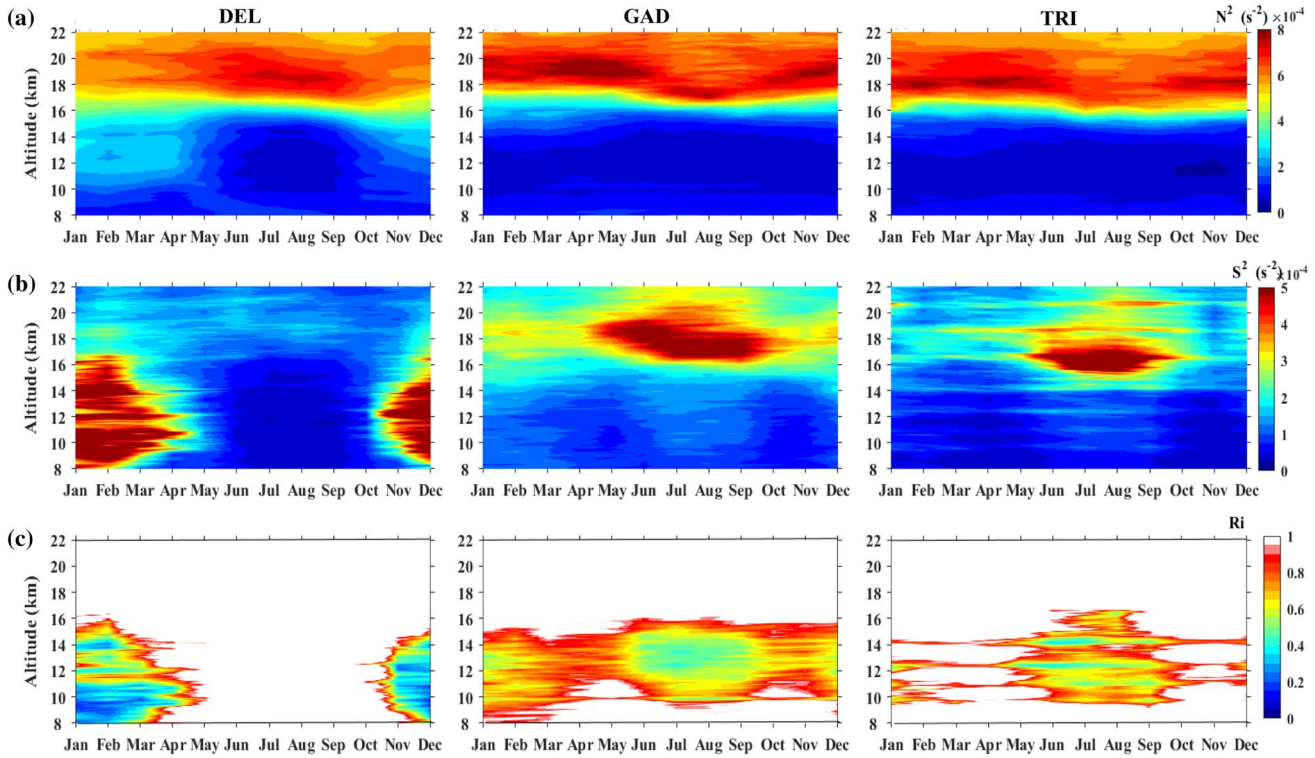

Fig. 8 Climatology of **a** stability parameter (N^2), **b** vertical shear of horizontal wind (S^2), and **c** Richardson number (Ri) for the stations: (first panel) DEL (Jan. 2004–Dec. 2016), (middle panel) GAD (Apr. 2006–Apr. 2017), and (last panel) TRI (Jan. 2004–Dec. 2016)

4.3 Role of vertical transport

Figure 9a shows the mean latitude–altitude distribution of vertical velocity during boreal summer. Uma et al. (2014) have extensively used the ERA-Interim vertical velocity up to the lower stratosphere over various monsoon regions and found to be reliable in terms of direction. The vertical velocity is averaged from 60°E to 80°E. Strong updrafts are observed between the equator and 25°N during boreal summer, extending up to the tropopause. In the region of strong updrafts, air from the boundary layer is pumped up to the tropopause altitude, thus we expect low ozone and high CO in the VOT. But over this region (equator and 25°N), we observed high ozone in the VOT, which can also be in situ produced in the lower troposphere and pumped up to the tropopause. Further, we analyzed the relationship between CO, which is an unambiguous tropospheric tracer and ozone, which may be either of stratospheric origin or in situ produced in the troposphere. Fadnavis et al. (2010) and Hoor et al. (2002) used the CO–O_3 correlation to identify the in-mixing of the stratospheric air into the troposphere and vice-versa, respectively. Figure 9b shows the scatter plot between O_3 and CO measured with the MLS. Scatter plots are obtained from time-series of monthly mean data sets at 100 hPa and averaged over the region between 0°–10°N and 60°E–80°E. During June to September, we observed high ozone (> 120 ppbv) with low CO (< 65 ppbv). Fishman and Seiler (1983) suggested that a positive correlation between CO and O_3 indicates in situ ozone production in the troposphere and negative correlation indicates ozone of stratospheric origin. Park et al. (2007) studied the statistical characterization of stratosphere and tropospheric air masses focusing over the ASM region on the basis of CO–O_3 correlation at 100 hPa. They concluded that air masses with in the ASM anticyclone shows mainly tropospheric signature while rest of the tropics generally shows mixed characteristics. The above mentioned studies characterized CO–O_3 relation on a time scale of days. In the present observation (Fig. 9b) we focused on the air mass characteristics over the study region (0–10°N, and 60°E–80°E) during JJAS and how it differ from other seasons. Figure 9b suggests that the observed enhancement in ozone in the VOT is of stratospheric origin i.e. transported from the NH mid-latitudes.

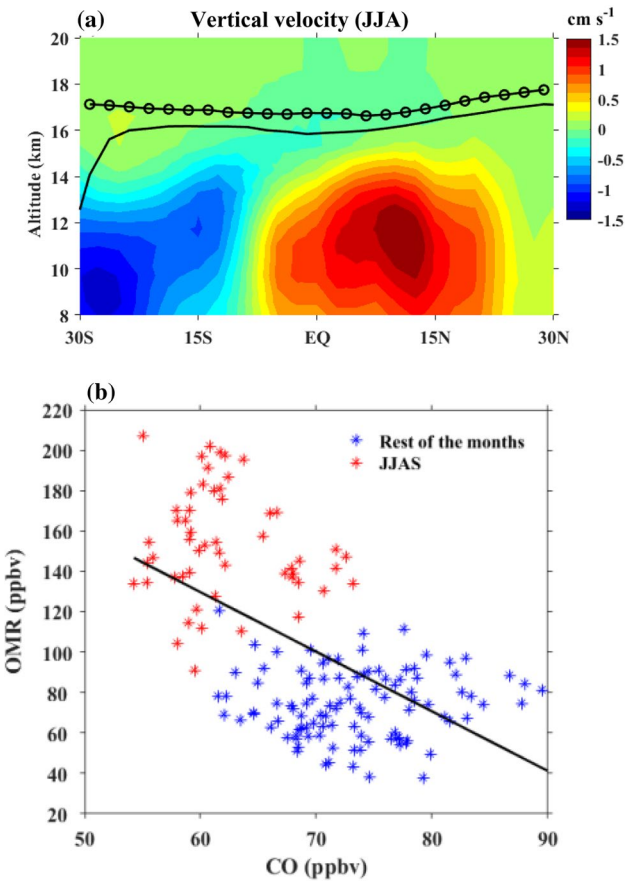

Fig. 9 **a** Latitude–altitude distribution of seasonal mean vertical velocity in cm s^{-1}, observed during boreal summer from ERA-Interim reanalysis. Data is averaged for the region 60°E and 80°E. **b** Scatter plot between ozone and carbon monoxide (CO) at 100 hPa. Data are monthly means from 2005 to 2017 and averaged for the region 0°–10°N, and 60°E–80°E. Red stars in Fig. 9b indicate the months of June–July–August–September (JJAS) and blue stars indicate remaining months. The black line shows the linear fit of entire data (r = 0.57)

4.4 Role of tropical tropopause

Figure 10 shows the seasonal mean lapse-rate (left) and cold-point (right) tropopause altitude (LRT-A, CPT-A), temperature (LRT-T, CPT-T), and pressure (LRT-P, CPT-P), for boreal summer. We observed highest tropopause altitude (LRT-A: 17–17.5 km and CPT-A: 17.5–18 km) inside the ASM anticyclone and lowest (LRT-A: 15.5–16 km and CPT-A: 16–16.5 km) over the equatorial Indian Ocean. The seasonal characteristics observed in the present analysis and the difference between the CPT and LRT are as similar as reported by Kim and Son (2012) and Munchak and Pan (2014), respectively. Higher tropopause over the TP is reported by Feng et al. (2011) and it is attributed to the presence of ASM anticyclone. The mean CPT-A over the NH is found to be 0.25 km higher as compared to SH. Similarly, we observed lowest CPT-P (< 90 hPa) over the TP and highest CPT-P (> 100 hPa) over the equatorial Indian Ocean. Interestingly, we also observed lower CPT-A, and higher CPT-P along the path of TEJ. Colder CPT-T is observed over the convectively active regions. The tropopause separates the ozone rich stratospheric air from the ozone poor tropospheric air and thus the ozone concentration in the UTLS region is expected to follow the tropopause structure. It is to be noted that high ozone concentration (~ 180

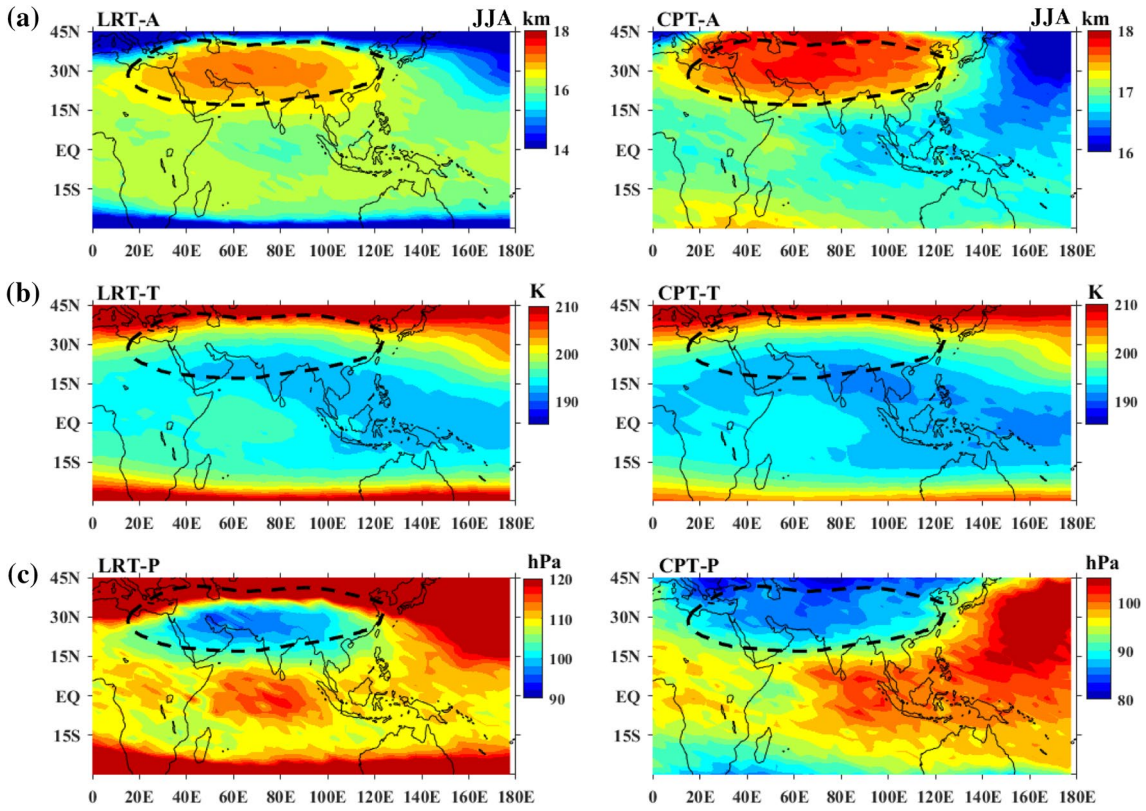

Fig. 10 Latitude–longitude distribution of lapse-rate tropopause (LRT) (left) and cold-point tropopause (CPT) (right) **a** altitude (-A), **b** temperature (-T), and **c** pressure (-P) observed during boreal summer

ppbv) is observed in the VOT between the equator and 10°N. The CPT is also found to be lowest between the equator and 10°N, where the core of the 'ozone river' located. Toward east (west) of ozone enhancement region over the Indian peninsula, the CPT-A (CPT-T) is lower (higher) by 0.2–0.3 km (2–3 K). The region of ozone enhancement (> 60 ppbv), low CPT-A (< − 0.6 km), and high CPT-T (> 3 K) are strongly correlated and overlapped between 140°E and 180°E, and 10°N and 30°N. This is also the region where the ozone transport from the sub-tropical stratosphere to the tropical upper troposphere originates (e.g., Konopka et al. 2010).

In order to verify the ozone presence over the southern India and tropical Indian Ocean, which is hypothesized to be the transport from mid-latitude, we correlate the daily fields of ozone at two regions, R1 and R2. R1 is averaged of 0°–10°N and 60°–80°E, and R2 is averaged of 15°–25°N and 120°–140°E. Figure 11a shows the scatter plot of mean removed ozone in the VOT at R1 and R2 during June to September. The analysis is carried out for time-series of daily mean data sets. A good positive correlation is observed, suggesting the high ozone over the R1 region is mostly transported from R2. Further the correlation between ozone and easterly wind over the R1 region shows that the amount of ozone is increasing with the intensity of zonal wind (Fig. 11b). It is to be noted that the intensity of easterly wind at R1 region (known as TEJ) is significantly controlled by ASM anticyclone (Sathiyamoorthy et al. 2007) and transport of ozone over the Indian peninsula is also controlled by the same anticyclone. About 50 ppbv of ozone can be increased with the increase of easterly wind intensity by 10 m s^{-1}. Thus, as the intensity of anticyclone increases both the phenomena are affected. As the tropopause is the barrier for the ozone transport, we also correlate the ozone with the tropopause altitude. It is clear from Fig. 11c, d that as the tropopause altitude decreases, the amount of ozone increases. Thus, undulation of tropopause may also contribute to the increase of ozone. It is found that about 50 ppbv of ozone can be increased with the decrease of tropopause by 1 km. The total ozone increases over the southern India and tropical Indian Ocean is about 180 ppbv and thus about 130 ppbv is mainly contributed due to the transport from the mid-latitude. However, a detail quantitative analysis is needed by launching series of ozonesonde observations along the path of anticyclone and TEJ.

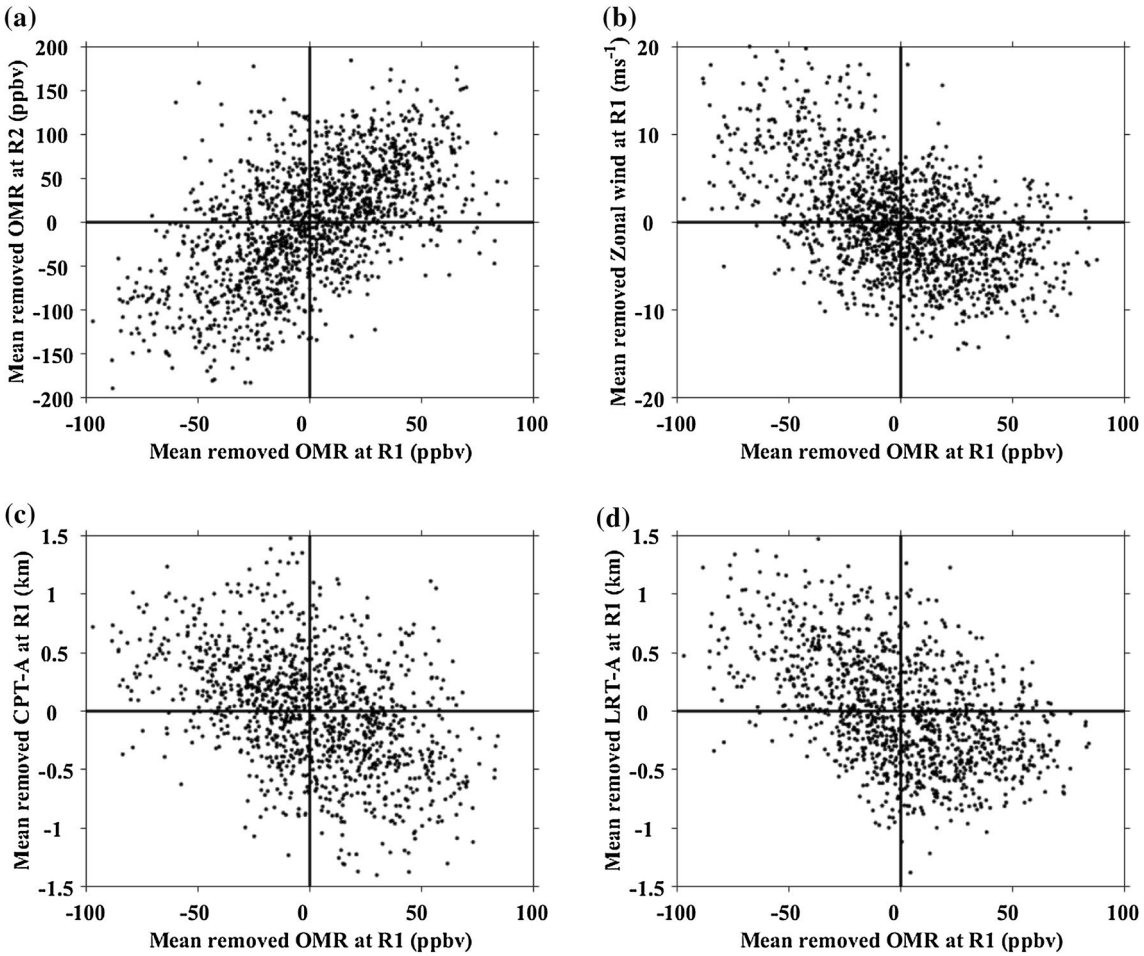

Fig. 11 Scatter plot of mean removed (JJAS) 100 hPa ozone at region 1 (R1) with **a** mean removed 100 hPa ozone at region 2 (R2), **b** mean removed zonal wind at 150 hPa, **c** mean removed CPT-A, and **d** mean removed LRT-A. R1 is averaged for 0°–10°N and 60°–80°E, and R2 is averaged for 15°–25°N and 120°–140°E. The data is daily mean from 1 June to 30 September of each year from 2005 to 2017 for ozone and 2007 to 2016 for tropopause

4.5 Estimation of mean mass-flux

The details of mass-exchange across the tropical tropopause are extremely important for understanding the consequence of chemical species fluxes in the UTLS. Thus, we estimate monthly mean mass-flux following the methodology introduced by Wei (1987). The basic idea of this method is to define tropopause as a material surface and to calculate mass per unit area across the surface. Thus in this method, vertical and horizontal movement of air across and along the tropopause respectively, and the temporal movement of tropopause surface are considered. The total mass-flux across the tropical tropopause in isobaric coordinates is given by Eq. (6) (Wei 1987).

$$F = \frac{1}{g}\left(-\omega + \boldsymbol{V}_h \cdot \nabla P_t + \frac{\partial P_t}{\partial t}\right) \tag{6}$$

Where g is the acceleration due to gravity (m s^{-2}), ω vertical velocity in pressure coordinate (Pa s^{-1}), $\boldsymbol{V}_h$ is the horizontal vector wind (m s^{-1}), and P_t is the tropopause pressure (Pa). The first and second terms (right-hand side) in Eq. (6) represents the exchange associated with the vertical and horizontal air motion, respectively, in the VOT. This term arises due to the pressure gradient exists along the tropopause. The third term quantifies the exchange arise due to the tropopause pressure variation with respect to time. The first two terms are calculated from instantaneous measurements while the third one is calculated at the discrete times. In the present analysis, we used the tropopause pressure obtained from the COSMIC measurements to estimate the mass-flux across the tropopause with a coarse spatial (10° latitude × 20° longitude) and temporal (1 day) resolution. The daily mean three components of wind at 100 hPa level are taken from the ERA-Interim reanalysis. Figure 12 shows the daily mean (smoothed by 5 day running mean)

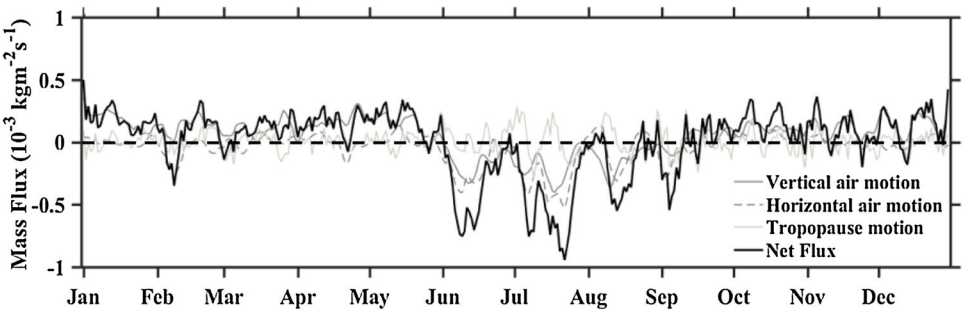

Fig. 12 Daily mean (smoothed by 5-day running mean) cross-tropopause mass-flux due to vertical motion, horizontal motion, tropopause motion and net-flux over 5°N–5°S, 60°E–80°E. Data is a composite of 9 years (2007–2015)

cross-tropopause mass flux due to vertical air motion, horizontal air motion, tropopause motion, and net flux. The monthly mean data is a composite of 9 years from 2007 to 2015 averaged of 5°N–5°S, and 60°E–80°E. A positive flux indicates the transport of mass from the troposphere to the stratosphere and vice-versa. Highest net-downward flux is observed during boreal summer and found between 0.75×10^{-3} and 1×10^{-3} kg m^{-2} s^{-1}. The net-downward mass flux during summer is contributed by both horizontal and vertical motion. The contribution of tropopause motion is very less as compared to horizontal and vertical motion. The observed downward mass-flux during boreal summer could be associated with the transport due to the anticyclone formation and direct stratospheric intrusion.

5 Summary

We use 14 years of ozone, water vapour and carbon monoxide observations from Aura-MLS and 11 years of tropopause data from the COSMIC temperature profiles, to understand the causative mechanism for the high upper tropospheric and lower stratospheric ozone over the tropical Indian region during Asian Summer monsoon (ASM) season. The observations are also supplemented with long-term in situ ozonesonde observations along with reanalysis data. High ozone concentration is observed in the upper troposphere and lower stratosphere (UTLS) over the tropical Indian region (southern India and tropical Indian Ocean), i.e. southernmost edges of the ASM anticyclone. Role of horizontal motion, monsoon convection, direct stratospheric intrusion due to turbulence, and tropical tropopause in the distributions of ozone over the ASM region are examined in detail. The horizontal transport follows the path of tropical easterly jet. The concentration of ozone increases with the intensity of the easterly jet, which indicates that the Asian Summer Monsoon anticyclone is the controlling factor of high ozone in the tropical Indian region. During boreal summer enhanced stability parameter is observed in the vicinity of tropopause along with strong wind shear and Richardson number less than 1, suggesting the possibility of dynamical stability. This instability may have a minor role in mixing the stratospheric air with the tropospheric air. Analysis of backward trajectories and CO–O_3 relation in the vicinity of tropopause clearly indicates that ozone observed over the southern India and tropical Indian Ocean regions are of stratospheric origin from the NH mid-latitudes. We estimated the net-downward mass flux of 0.75×10^{-3} to 1×10^{-3} kg m^{-2} s^{-1} during summer.

It is envisaged that the present study will have an important implications as ozone distributions in the UTLS region influences the balance of Earth's radiation and chemistry over the ASM region. However, further analysis is needed with many more ozonesonde observations along the path of ASM anticyclone to quantify the contributions by various factors.

Acknowledgements Authors would like to acknowledge Goddard Earth Sciences Data and Information Services Centre and UCAR/CDAAC team for providing the Aura-MLS and COSMIC data, respectively. Thanks are also due to ECMWF for providing the ERA-Interim and India Meteorological Department for ozonesonde data. One of the author KVS thankful to Indian Space Research Organization (ISRO) for providing doctoral fellowship during this study period. Author gratefully acknowledges both the reviewers and Editor for their valuable comments and suggestions for the improvement of the manuscript. The gridded data used in the present study can be obtained on request.

References

Alexander G, Chatterjee K (1980) Atmospheric ozone measurements in India. Proc Indian Natl Sci Acad 46:234–244

Alexander P, Torre A, Llamedo P, Hierro R (2014) Precision estimation in temperature and refractivity profiles retrieved by GPS radio occultations. J Geophys Res 119:8624–8638. https://doi.org/10.1002/2013JD021016

Baray JL, Ancellet G, Randriambelo T, Baldy S (1999) Tropical cyclone Marlene and stratosphere–troposphere exchange. J Geophys Res 104:13953–13970. https://doi.org/10.1029/1999JD900028

Bian J, Pan LL, Paulik L, Vömel H, Chen H, Lu D (2012) In situ water vapor and ozone measurements in Lhasa and Kunming during the Asian summer monsoon. Geophys Res Lett 39:L19808. https://doi.org/10.1029/2012GL052996

Bourqui MS, Trepanier PY (2010) Descent of deep stratospheric intrusions during the IONS August 2006 campaign. J Geophys Res 115:D18301. https://doi.org/10.1029/2009JD013183

Cairo F, Buontempo C, MacKenzie AR, Schiller C, Volk CM, Adriani A, Mitev V, Matthey R, Di Donfrancesco G, Oulanovsky A, Ravegnani F, Yushkov V, Snels M, Cagnazzo C, Stefanutti L (2008) Morphology of the tropopause layer and lower stratosphere above a tropical cyclone: a case study on cyclone Davina (1999). Atmos Chem Phy 8:3411–3426. https://doi.org/10.5194/acp-8-3411-2008

Chakrabarty DK, Shah NC, Pandya KV, Peshin SK (2000) Long term trend of tropopause over New Delhi and Thiruvananthapuram. Geophys Res Lett 27(2184):2181. https://doi.org/10.1029/2000GL011463

Das SS (2009) A new perspective on MST radar observations of stratospheric intrusions into troposphere associated with tropical cyclone. Geophys Res Lett 36:L15821. https://doi.org/10.1029/2009GL039184

Das SS, Sijikumar S, Uma KN (2011) Further investigation on stratospheric air intrusion into the troposphere during the episode of tropical cyclone: numerical simulation and MST radar observations. Atmos Res 101:928–937. https://doi.org/10.1016/j.atmosres.2011.05.023

Das SS, Ratnam MV, Uma KN, Patra AK, Subrahmanyam KV, Girach IA, Suneeth KV, Kumar KK, Ramkumar G (2016a) Stratospheric intrusion into the troposphere during the tropical cyclone Nilam (2012). Q J R Meteorol Soc 142:2168–2179. https://doi.org/10.1002/qj.2810

Das SS, Ratnam MV, Uma KN, Subrahmanyam KV, Girach IA, Patra AK, Aneesh S, Suneeth KV, Kumar KK, Kesarkar AP, Sijikumar S, Ramkumar G (2016b) Influence of tropical cyclones on tropospheric ozone: possible implications. Atmos Chem Phys 16:1–11. https://doi.org/10.5194/acp-16-1-2016

Das SS, Uma KN, Bineesha VN, Suneeth KV, Ramkumar G (2016c) Four decadal climatological intercomparison of Rocketsonde and Radiosonde with different reanalysis data: results from Thumba Equatorial Station. Q J R Meteorol Soc 142:91–101. https://doi.org/10.1002/qj.2632 doi

Davies TD, Schuepbach E (1994) Episodes of high ozone concentration at the earth's surface resulting from transport down from the upper troposphere–lower stratosphere: a review and case studies. Atmos Environ 28:53–68. https://doi.org/10.1016/1352-2310(94)90022-1

Dee DP, Uppala SM, Simmons AJ, Berrisford P, Poli P, Kobayashi S, Andrae U, Balmaseda MA, Balsamo G, Bauer P, Bechtold P, Beljaars ACM, van de Berg L, Bidlot J, Bormann N, Delsol C, Dragani R, Fuentes M, Geer AJ, Haimberger L, Healy SB, Hersbach H, H´olm EV, Isaksen L, K°allberg P, K¨ohler M, Matricardi M, McNally AP, Monge-Sanz BM, Morcrette J-J, Park B-K, Peubey C, de Rosnay P, Tavolato C, Th´epaut J-N, Vitart F (2011) The ERA-Interim reanalysis: configuration and performance of the data assimilation system. Q J R Meteorol Soc 137:553–597. https://doi.org/10.1002/qj.828

Deshler T, Mercer JL, Smit HGJ, Stubi R, Levrat G, Johnson BJ, Oltmans SJ, Kivi R, Thompson AM, Witte J, Davies J, Schmidlin FJ, Brothers G, Sasaki T (2008) Atmospheric comparison of electrochemical cell ozonesondes from different manufacturers, and with different cathode solution strengths: the Balloon Experiment on Standards for Ozone sondes. J Geophys Res 113:D04307. https://doi.org/10.1029/2007JD008975

Duan AM, Wu GX (2005) Role of the Tibetan Plateau thermal forcing in the summer climate patterns over subtropical Asia. Clim Dyn 24:793. https://doi.org/10.1007/s00382-004-0488-8

Dunkerton TJ (1995) Evidence of meridional motion in the summer lower stratosphere adjacent to monsoon regions. J Geophys Res 100:16675–16688. https://doi.org/10.1029/95JD01263

Fadnavis S, Chakraborty T, Beig G (2010) Seasonal stratospheric intrusion of ozone in the upper troposphere over India. Ann Geophys 28:2149–2159. https://doi.org/10.5194/angeo-28-2149-2010

Fadnavis S, Dhomse S, Ghude S, Iyer U, Buchunde P, Sonbawne S, Raj PE (2012) Ozone trends in the vertical structure of upper troposphere and lower stratosphere over the Indian monsoon region. Int J Environ Sci Technol. https://doi.org/10.1007/s13762-013-0258-4

Feng S, Fu Y, Xiao Q (2011) Is the tropopause higher over the Tibetan Plateau? Observational evidence from Constellation Observing System for Meteorology, Ionosphere, and Climate (COSMIC) data. J Geophys Res 116:D21121. https://doi.org/10.1029/2011JD016140

Fishman J, Seiler W (1983) Correlative nature of ozone and carbon monoxide in the troposphere: implications for the tropospheric ozone budget. J Geophys Res 88(C6):3662–3670. https://doi.org/10.1029/JC088iC06p03662

Fu R, Hu Y, Wright JS, Jiang JH, Dickinson RE, Chen M, Filipiak M, Read WG, Waters JW, Wu DL (2006) Short circuit of water vapor and polluted air to the global stratosphere by convective transport over the Tibetan Plateau. Proc Natl Acad Sci USA 103:5664–5669. https://doi.org/10.1073/pnas.0601584103

Gettelman A, Forster PMdeF, Fujiwara M, Fu Q, Vömel H, Gohar LK, Johanson C, Ammerman M (2004) Radiation balance of the tropical tropopause layer. J Geophys Res 109:D07103. https://doi.org/10.1029/2003JD004190

Glanville A, Birner T (2017) Role of vertical and horizontal mixing in the tape recorder signal near the tropical tropopause. Atmos Chem Phys 17:4337–4353. https://doi.org/10.5194/acp-17-4337-2017

Hajj GA, Ao CO, Iijima BA, Kuang D, Kursinski ER, Mannucci AJ, Meehan TK, Romans LJ, de la Torre Juarez M, Yunck TP (2004) CHAMP and SAC-C atmospheric occultation results and intercomparison. J Geophys Res 109:06109. https://doi.org/10.1029/2003JD003909

Holton JR, Haynes PT, Mclntyre ME (1995) Stratosphere–troposphere exchange. Rev Geophys 33:403:439. https://doi.org/10.1029/95RG02097

Hoor P, Fischer H, Lange L, Lelieveld J, Brunner D (2002) Seasonal variations of mixing layer in the lowermost stratosphere as identified by the CO–O_3 correlation from in situ measurements. J Geophys Res 107D(5):4044. https://doi.org/10.1029/2000JD000289

Jacobson MZ (2005) Fundamental of atmospheric modeling. Cambridge University Press, New York **(ISBN-13 978-o-511-11115-o)**

Jiang YC, Zhao TL, Liu J, Xu XD, Tan CH, Cheng XH, Bi XY, Gan JB, You JF, Zhao SZ (2015) Why does surface ozone peak before a typhoon landing in southeast China? Atmos Chem Phys 15:13331–13338. https://doi.org/10.5194/acp-15-13331-2015

Johnson FS (1975) Transport processes in the upper atmosphere. J Atmos Sci 32:1658–1662. https://doi.org/10.1175/1520-0469(1975)032%3C1658:TPITUA%3E2.0.CO;2

Kerr JB, Fast H, McElroy CT, Oltmans SJ, Lathrop JA, Kyro E, Paukkunen A, Claude H, Köhler U, Sreedharan CR, Takao T, Tsukagoshi Y (1994) The 1991 WMO international ozonesonde intercomparison at Vanscoy. Can Atmos Ocean 32:685–716. https://doi.org/10.1080/07055900.1994.9649518

Kim J, Son SW (2012) Tropical Cold-point tropopause: climatology, seasonal cycle, and intraseasonal variability derived from COSMIC GPS radio occultation measurements. J Clim 25:5343–5360. https://doi.org/10.1175/JCLI-D-11-00554.1

Kim YK, Lee HW, Park JK, Moon YS (2002) The stratosphere–troposphere exchange of ozone and aerosols over Korea. Atmos Environ 36:449–463. https://doi.org/10.1016/S1352-2310(01)00370-3

Kizu N, Sugidachi T, Kobayashi E, Hoshino S, Shimizu K, Maeda R, Fujiwara M (2018) Technical characteristics and GRUAN data processing for the Meisei RS-11G and iMS-100 radiosondes, GRUAN-TD-5, p 152. https://www.gruan.org/documentation/gruan/td/graun-td-5/

Komhyr WD, Barnes RA, Brothers GB, Lathrop JA, Opperman DP (1995) Electrochemical concentration cell ozonesonde

performance evaluation during STOIC 1989. J Geophys Res 100:9231–9244. https://doi.org/10.1029/94JD02175

Konopka P, Grooß JU, Gunther G, Ploeger F, Pommrich R, Muller R, Livesey N (2010) Annual cycle of ozone at and above the tropical tropopause: observations versus simulations with the Chemical Lagrangian Model of the Stratosphere (CLaMS). Atmos Chem Phys 10:121–132. https://doi.org/10.5194/acp-10-121-2010

Kucharski F, Bracco A, Barimalala R, Yoo JH (2010) Contribution of the east–west thermal heating contrast to the South Asian monsoon and consequences for its variability. Clim Dyn 37:721–735. https://doi.org/10.1007/s00382-010-0858-3

Kursinski ER, Hajj GA, Schofield JT, Linfield RP, Hardy KR (1997) Observing Earth's atmosphere with radio occultation measurements using the global positioning system. J Geophys Res 102:23429–23465. https://doi.org/10.1029/97JD01569

Lal S, Venkataramani S, Chandra N, Cooper OR, Brioude J, Naja M (2014) Transport effects on the vertical distribution of tropospheric ozone over western India. J Geophys Res 119:10012–10026. https://doi.org/10.1002/2014JD021854

Lambert A, Read W, Livesey N (2015) MLS/Aura Level 2 water vapor (H_2O) mixing ratio V004, Greenbelt, MD, USA, Goddard Earth Sciences Data and Information Services Center (GES DISC). https://doi.org/10.5067/Aura/MLS/DATA2009

Lau M, Kim MK, Kim M (2006) Asian summer monsoon anomalies induced by aerosol direct forcing: the role of the Tibetan Plateau. Clim Dyn 26:855–864. https://doi.org/10.1007/s00382-006-0114-z

Liu YM, Wu GX, Liu H, Liu P (2001) Condensation heating of the Asian summer monsoon and the subtropical anticyclone in the Eastern Hemisphere. Clim Dyn 17:327–338. https://doi.org/10.1007/s003820000117

Liu Y, Wu G, Hong J, Dong B, Duan A, Bao Q, Zhou L (2012) Revisiting Asian monsoon formation and change associated with Tibetan Plateau forcing: II. Change Clim Dyn 39:1183. https://doi.org/10.1007/s00382-012-1335-y

Livesey NJ, Read WG, Wagner PA, Froidevaux L, Lambert A, Manney GL, Valle LFM, Pumphrey HC, Santee ML, Schwartz MJ, Wang S, Fuller RA, Jarnot RF, Knosp BW, Martinez E (2015) Earth Observing System (EOS) Aura Microwave Limb Sounder (MLS) version V4.2x level 2 data quality and description document. Jet Propul Lab Pasadena, CA. JPL D-33509 Rev. A. http://mls.jpl.nasa.gov

Munchak LA, Pan LL (2014) Separation of the lapse rate and the cold point tropopauses in the tropics and the resulting impact on cloud top tropopause relationships. J Geophys Res 119:7963–7978. https://doi.org/10.1002/2013JD021189

Murphy EA, D'agostino RB, Noonan JP (1982) Patterns in the occurrence of Richardson numbers less than unity in the lower atmosphere. J Appl Meteorol 21:321–333. https://doi.org/10.1175/1520-0450(1982)021%3C0321:PITOOR%3E2.0.CO;2

Nash J, Oakley T, Vomel H, Wei L (2011) WMO Intercomparison of High Quality Radiosonde Systems Yangjiang, China, 12 July – 3 August 2010, Technical report, WMO/TD-No. 1580, instruments and observing methods Report, No. 107. https://www.wmo.int/pages/prog/www/IMOP/publications/IOM-107_Yangjiang/IOM 107_Yangjiang.zip, https://library.wmo.int/opac/index.php?lvl=notice_display&id=15531#

Ojha N, Naja M, Sarangi T, Kumar R, Bhardwaj P, Lal S, Venkataramani S, Sagar R, Kumar A, Chandola HC (2014) On the processes influencing the vertical distribution of ozone over the central Himalayas: analysis of yearlong ozonesonde observations. Atmos Environ 88:201–211. https://doi.org/10.1016/j.atmosenv.2014.01.031

Pan LL, Homeyer CR, Honomichl S, Ridley BA, Weisman M, Barth MC, Hair JW, Fenn MA, Butler C, Diskin GS, Crawford JH, Ryerson TB, Pollack I, Peischl J, Huntrieser H (2015) Thunderstorms enhance tropospheric ozone by wrapping and shedding stratospheric air. Geophy Res Lett 41:7785–7790. https://doi.org/10.1002/2014gl061921

Park M, Randel WJ, Kinnison DE, Garcia RR, Choi W (2004) Seasonal variation of methane, water vapor, and nitrogen oxides near the tropopause: satellite observations and model simulations. J Geophys Res 109:D03302. https://doi.org/10.1029/2003JD003706

Park M, Randel WJ, Gettelman A, Massie ST, Jiang JH (2007) Transport above the Asian summer monsoon anticyclone inferred from Aura Microwave Limb Sounder tracers. J Geophys Res 112:D16309. https://doi.org/10.1029/2006JD008294

Raj STA, Venkat Ratnam M, Rao DN, Krishna Murthy BV (2015) Vertical distribution of ozone over a tropical station: seasonal variation and comparison with satellite (MLS, SABER) and ERA-Interim products. Atmos Environ 116:281–292. https://doi.org/10.1016/j.atmosenv.2015.06.047

Raman RM, Rao VVMJ, Ratnam MV, Rajeevan M, Rao SVB, Rao DN, Rao NP (2009) Characteristics of the tropical easterly jet: long-term trends and their features during active and break monsoon phases. J Geophys Res 114:D19105. https://doi.org/10.1029/2009JD012065

Randel WJ, Jensen EJ (2013) Physical processes in the tropical tropopause layer and their roles in a changing climate. Nat Geosci 6:169–176. https://doi.org/10.1038/ngeo1733

Randel WJ, Park M (2006) Deep convective influence on the Asian summer monsoon anticyclone and associated tracer variability observed with AIRS. J Geophys Res 111:D12314. https://doi.org/10.1029/2005JD006490

Randel WJ, Wu F (2015) Variability of zonal mean tropical temperatures derived from a decade of GPS radio occultation data. J Atmos Sci 72:1261–1275. https://doi.org/10.1175/JAS-D-14-0216.1

Randel WJ, Wu F, Vömel H, Nedoluha GE, Forster P (2006) Decreases in stratospheric water vapor after 2001: links to changes in the tropical tropopause and the Brewer–Dobson circulation. J Geophys Res 111:D12312. https://doi.org/10.1029/2005JD006744

Randel WJ, Park M, Wu F, Livesey N (2007) A large annual cycle in ozone above the tropical tropopause linked to the Brewer–Dobson circulation. J Atmos Sci 64:4479–4488, doi

Saraf N, Beig G (2004) Long-term trends in tropospheric ozone over the Indian tropical region. Geophys Res Lett 31:L05101. https://doi.org/10.1029/2003GL018516

Sathiyamoorthy V, Pal PK, Joshi PC (2007) Intraseasonal variability of the tropical easterly jet. Meteorol Atmos Phys 96:305–316. https://doi.org/10.1007/s00703-006-0214-7

Schwartz M, Froidevaux L, Livesey N, Read W (2015) MLS/Aura Level 2 ozone (O_3) mixing ratio V004, Greenbelt, MD, USA, Goddard Earth Sciences Data and Information Services Center (GES DISC). https://doi.org/10.5067/Aura/MLS/DATA2017

Škerlak B, Sprenger M, Wernli H (2014) A global climatology of stratosphere–troposphere exchange using the ERA-Interim data set from 1979 to 2011. Atmos Chem Phys 14:913–937. https://doi.org/10.5194/acp-14-913-2014

Sprenger M, Wernli H (2003) A northern hemispheric climatology of cross-tropopause exchange for the ERA15 time period (1979–1993). J Geophys Res 108:D12. https://doi.org/10.1029/2002JD002636

Sreedharan CR (1968) An Indian electrochemical ozonesonde. J Phys E Sci Inst Sr 2:995–997

Stein AF, Draxler RR, Rolph GD, Stunder BJB, Cohen MD, Ngan F (2015) NOAA's HYSPLIT atmospheric transport and dispersion modeling system. Bull Am Meteorol Soc 96:2059–2077. https://doi.org/10.1175/BAMS-D-14-00110.1

Steinbrecht W, Claude H, Schonenborn F, Leiterer U, Dier H, Lanzinger E (2008) Pressure and temperature differences between

Vaisala RS80 and RS92 radiosonde systems. J Atmos Ocean Tech 25:909–927. https://doi.org/10.1175/2007JTECHA999.1

Stohl A, Wernli H, Bourqui M, Forster C, James P, Liniger MA, Seibert P, Sprenger M (2003) A new perspective of stratosphere–troposphere exchange. Bull Am Meteorol Soc 84:1565–1573. https://doi.org/10.1175/BAMS-84-11-1565

Stolarski RS, Waugh DW, Wang L, Oman LD, Douglass AR, Newman PA (2014) Seasonal variation of ozone in the tropical lower stratosphere: southern tropics are different from northern tropics. J Geophys Res 119:6196–6206. https://doi.org/10.1002/2013JD021294

Suneeth KV, Das SS, Das SK (2017) Diurnal variability of the global tropical tropopause: results inferred from COSMIC observations. Clim Dyn 49:3277–3292. https://doi.org/10.1007/s00382-016-3512-x

Tian W, Tian H, Dhomse S, Feng W (2011) A study of upper troposphere and lower stratosphere water vapor above the Tibetan Plateau using AIRS and MLS data. Atmos Sci Lett 12:233–239. https://doi.org/10.1002/asl.319

Tobo Y, Iwasaka Y, Zhang D, Shi G, Kim YS, Tamura K, Ohashi T (2008) Summertime "ozone valley" over the Tibetan Plateau derived from ozonesondes and EP/TOMS data. Geophys Res Lett 35:L16801. https://doi.org/10.1029/2008GL034341

Uma KN, Das SK, Das SS (2014) A climatological perspective of water vapour at the UTLS region over different global monsoon regions: observations inferred from the AURA-MLS and reanalysis data. Clim Dyn 43:407–420. https://doi.org/10.1007/s0038-014-2085-9

Vaughan G, Price J (1989) Ozone transport into the troposphere in a cut-off low event, Ozone in the atmosphere. In: Bojkov R, Fabian P, Deepak A (eds) Publishing Hampton, USA, pp 415–418

Venkat Ratnam M, Babu SR, Das SS, Basha G, Krishnamurthy BV, Rao BV (2016) Effect of tropical cyclones on the stratosphere–troposphere exchange observed using satellite observations over north Indian Ocean. Atmos Chem Phys 16:8581–8591. https://doi.org/10.5194/acp-16-8581-2016

Wei MY (1987) A New formulation of the exchange of mass and trace constituents between the stratosphere and troposphere. J Atmos Sci 44:3079–3086, https://doi.org/10.1175/1520-0469(1987)044%3C3079:ANFOTE%3E2.0.CO;2

Wild O (2007) Modeling the global tropospheric ozone budget: exploring the variability in current models. Atmos Chem Phys 7:2643–2660. https://doi.org/10.5194/acp-7-2643-2007

Worden J et al (2009) Observed vertical distribution of tropospheric ozone during the Asian summertime monsoon. J Geophys Res 114:D13304. https://doi.org/10.1029/2008JD010560

Wu G, Liu Y, Dong B, Liang X, Duan A, Bao Q, Yu J (2012) Revisiting Asian monsoon formation and change associated with Tibetan Plateau forcing: I. Formation. Clim Dyn 39:1169. https://doi.org/10.1007/s00382-012-1334-z

Xu X, Zhao T, Lu C, Guo Y, Chen B, Liu R, Li Y, Shi X (2014) An important mechanism sustaining the atmospheric "water tower" over the Tibetan Plateau. Atmos Chem Phys 14:11287–11295. https://doi.org/10.5194/acp-14-11287-2014

Yanai M, Li CF, Song ZS (1992) Seasonal heating of the Tibetan Plateau and its effects on the evolution of the Asian summer monsoon. J Meteorol Soc Jpn 70:319–351. https://doi.org/10.2151/jmsj1965.70.1B_319

Zhan R, Wang Y (2012) Contribution of tropical cyclones to stratosphere–troposphere exchange over the northwest Pacific: estimation based on AIRS satellite retrievals and ERA-Interim data. J Atmos Res 117:D12112. https://doi.org/10.1029/2012JD017494

Zhou X, Luo C (1994) Ozone valley over Tibetan Plateau. Acta Meteorol Sin 8:505–506

Zou H (1996) Seasonal variation and trends of TOMS ozone over Tibet. Geophys Res Lett 23:1029–1032. https://doi.org/10.1029/96GL00767